Biochem. J. (2011) **437**, 345–355 (Printed in Great Britain) doi:10.1042/BJ20110520

online data

SUPPLEMENTARY ONLINE DATA

AW551984: a novel regulator of cardiomyogenesis in pluripotent embryonic cells

Satoshi YASUDA*, Tetsuya HASEGAWA*†, Tetsuji HOSONO*‡, Mitsutoshi SATOH†, Kei WATANABE*§, Kageyoshi ONO‖, Shunichi SHIMIZU§, Takao HAYAKAWA¶, Teruhide YAMAGUCHI**, Kazuhiro SUZUKI* and Yoji SATO*[1]

*Division of Cellular and Gene Therapy Products, National Institute of Health Sciences, 1-18-1 Kami-yoga, Setagaya-ku, Tokyo 158-8501, Japan, †Department of Toxicology and Pharmacology, Faculty of Pharmaceutical Sciences, Toho University, Miyama 2-2-1, Funabashi, Chiba 274-8510, Japan, ‡Laboratory of Medicinal Microbiology, Yokohama College of Pharmacy, 601 Matanocyo, Totsuka-ku, Yokohama, Kanagawa 245-0066, Japan, §Department of Pathophysiology, School of Pharmacy, Showa University, 1-5-8 Hatanodai, Shinagawa-ku, Tokyo 142-8555, Japan, ‖Laboratory of Pharmacology, School of Pharmaceutical Sciences, Teikyo University, 1091-1 Suwarashi, Midori-ku, Sagamihara, Kanagawa 252-5195, Japan, ¶Pharmaceutical Research and Technology Institute, Kinki University, 3-4-1 Kowakae, Higashi-Osaka, Osaka 577-8502, Japan, and **Division of Biological Chemistry and Biologicals, National Institute of Health Sciences, 1-18-1 Kami-yoga, Setagaya-ku, Tokyo 158-8501, Japan

See the following pages for Supplementary Figures S1–S4 and Supplementary Tables S1–S4.

[1]To whom correspondence should be addressed (email yoji@nihs.go.jp).

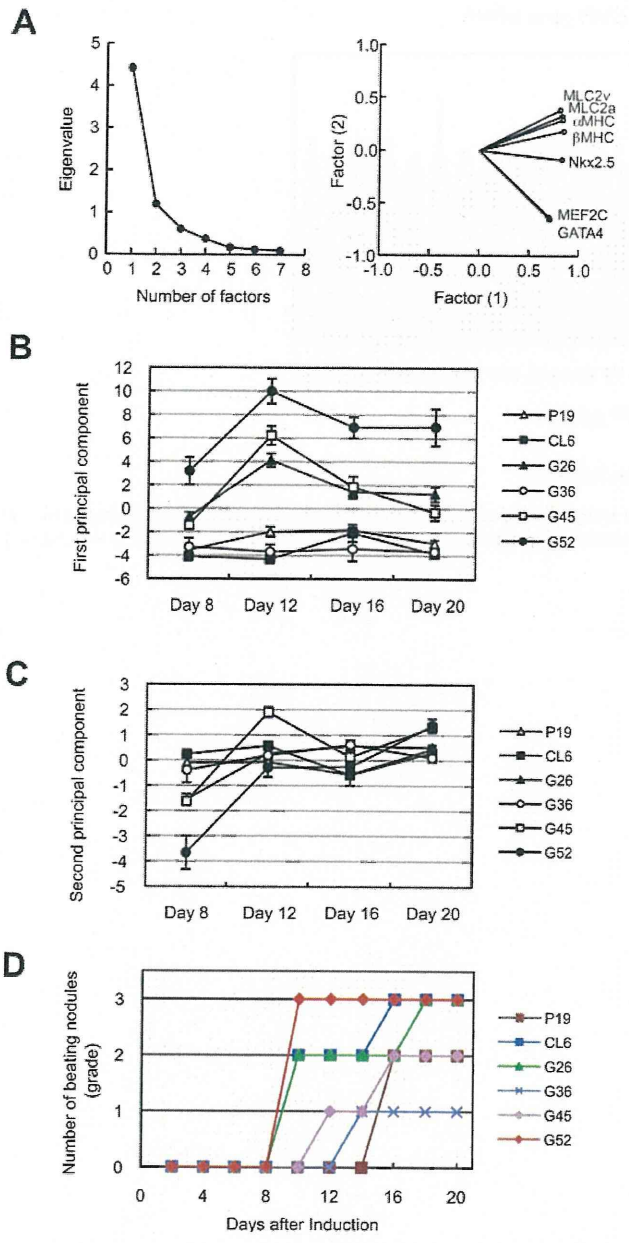

Figure S1 Cardiomyogenesis of P19 cells, P19CL6 cells and P19CL6 cell sublines

(**A–C**) PCA was performed using expression data of cardiac marker genes [*Nkx2.5*, *Gata4*, *Mef2c*, *Myh6* (α-MHC), *Myh7* (β-MHC), *Mlc2a* and *Mlc2v*] in differentiated P19 cells, P19CL6 cells and P19CL6 cell sublines (CL6G26, CL6G36, CL6G45 and CL6G52). (**A**) Scree plot indicates eigenvalues plotted against the factor numbers (left-hand panel). Factor loadings plot compares the two factor analyses (right-hand panel). (**B**) First component scores of P19 cells, P19CL6 cells and P19CL6 cell sublines at days 8, 12, 16 and 20. (**C**) Second component scores of P19 cells, P19CL6 cells and P19CL6 cell sublines at days 8, 12, 16 and 20. (**D**) P19 cells, P19CL6 cells and P19CL6 cell sublines (CL6G26, CL6G36, CL6G45 and CL6G52) were differentiated in the presence of 1 % DMSO. Nodules exhibiting spontaneous beating were counted with a microscope every other day and assessed non-parametrically, as described in the Materials and methods section of the main paper.

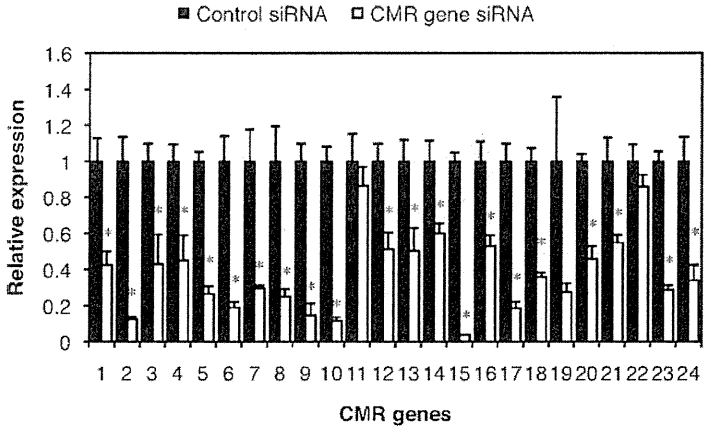

Figure S2 Efficiency of CMR gene knockdown by siRNA targeting the CMR genes in EC cells

CL6G52 cells were transfected with 100 nM siRNA targeting the CMR genes or the negative control siRNA. After 48 h, total RNA was isolated from the transfected cells. mRNA levels of the CMR genes were measured by qRT-PCR and normalized to 18S rRNA levels. Expression levels in cells transfected with the negative control were set to 1. Results are means $\pm$ S.E.M. ($n = 6$). Statistical significance was determined using a Student's t test (*$P < 0.05$ compared with control).

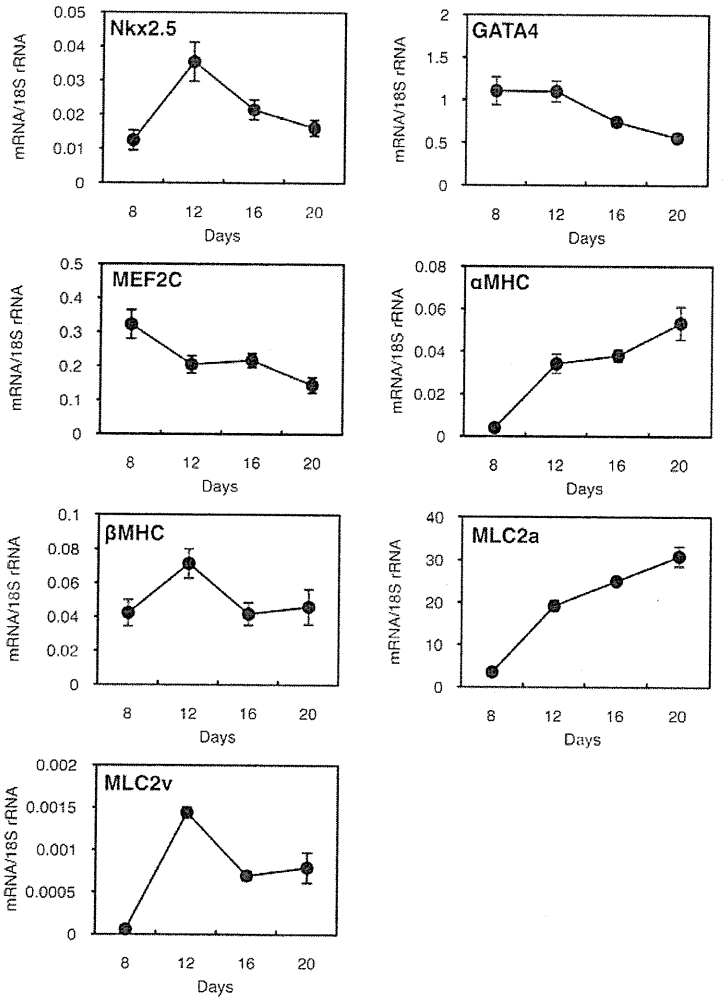

Figure S3 Transcript expression of cardiac marker genes in differentiated EC cells

An EC cell strain, CL6G52, was differentiated in the presence of 1 % DMSO. Total RNA was isolated from differentiated CL6G52 cells at days 8, 12, 16 and 20 and was subjected to one-step qRT-PCR. mRNA levels of *Nkx2.5*, *Gata4*, *Mef2c*, *Myh6* (α-MHC), *Myh7* (β-MHC), *Mlc2a* and *Mlc2v* were normalized to 18S rRNA levels. Results are means $\pm$ S.E.M. ($n = 6$).

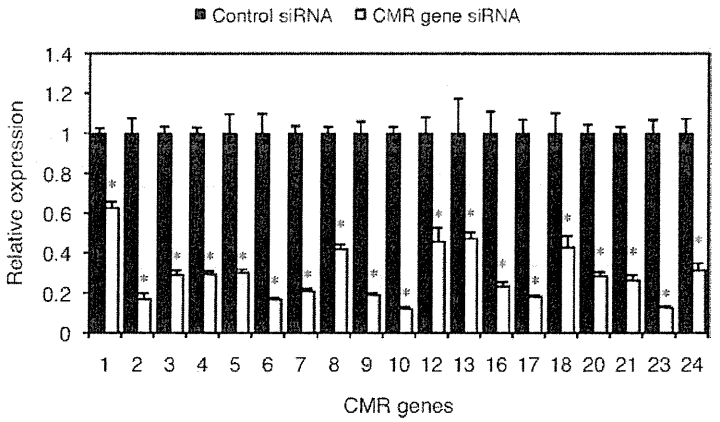

Figure S4 Efficiency of CMR gene knockdown by siRNA targeting the CMR genes in ES cells

R1 cells were transfected with 50 nM siRNA targeting the CMR genes or the negative control siRNA in the presence of 1000 units/ml LIF. After 24 h, total RNA was isolated from the transfected cells. mRNA levels of the CMR genes were measured by qRT-PCR and normalized to those of *Gapdh*. Expression levels in cells transfected with the negative control were set to 1. Results are means ± S.E.M. ($n = 5$). Statistical significance was determined using a Student's t test (*$P < 0.05$ compared with control).

Table S1 Probes and primers for qRT-PCR

Gene names are provided in the main paper.

Gene	Probe sequences (5′→3′)	Forward primer sequences (5′→3′)	Reverse primer sequences (5′→3′)
Nkx2.5	TGCTGAAGCTCACGTCCACGCAG	CTTCAAGCAACAGCGGTACCT	CGCTGTCGCTTGCACTTGTA
Gata4	TGCATCTCCTGTCACTCAGACATCGCA	TGCTCTAAGCTGTCCCCACAA	GTGATTATGTCCCCATGACTGTCA
Mef2c	CCAGTTACCATCCCAGTGTCCAGCCATAAC	TCCACCTCCCAGCTTTGAGAT	TGACAGGATTGCTGTACACCAAAC
Mlc2a	AAGGCCTTCAGCTGCATTGACCAGAAC	AAGCCCAGATTCAGGATTCAAG	AGCTCTTCCTCCGGAACACTT
Mlc2v	CATGGACCAGAACAGAGACGGCTTCA	GGAGTTCAAGGAAGCCTTCACA	TGTGTCCCTTAGGTCATTCTTGTC
Myh6 (α-MHC)	TCTGCTGATACCGGTGACAGTGGTAAAGG	CATGGCTACACTCTTCTCTACCTATGC	GGTGGAGAGCAGACACTGTTTG
Myh7 (β-MHC)	ACCCCTACGATTATGCGTTCATCTCCCAA	TTTCTACCAAATCCTGTCTAATAAAAAGC	GTCATCAATGGAGGCCACAGT
Nanog	ACTCCACTGGTGCTGAGCCCTTCTGA	CAGTGGTTGAAGACTAGCAATGG	GCTGCAATGGATGCTGGGA
Oct3/4	CCCGAGGAGTCCCAGGACATGAAAGC	CGTGAAGTTGGAGAAGGTGGAA	CCAAGGTGATCCTCTTCTGCTTC
T/brachyury	TGCCAGCACCAGGAACAAGCCACC	AGCAGCCGGGGTATTCCC	CTGAGGGTGGGAGCTGGC
Mesp1	AGCCCAGTCCCTCATCTCCGCTCTTC	CATCCCAGGAAAGGCAGGAAA	GCGGCGTCCAGGTTTCTAG
Tbx5	Mm00803518_m1 (Applied Biosystems)		

CMR gene	Probe sequences (5′→3′)	Forward primer sequences (5′→3′)	Reverse primer sequences (5′→3′)
Prdm5	CCACAGTGTGAATCGAGCTTTCCCAGTG	AGGTCACCTTGGCTGTGAAGA	CCGCAGTTCTCGCATTTGA
AW551984	CCGATGGACGTGAGGACAGTAATCTGGA	CCATCCTGAATCCTAGATACCATCTC	TAGTGGCAACCATGCTGAGTGT
D430028G21Rik	AGTGCACTCTTGGCTGTATTCCTGGCA	CCCCAAGAAGAGGAAGAACATTG	CGCCTACTACGGTACAGCATCA
5330410G16Rik	TCTCCCTTCGGTACCTGTTTTCCATGC	GGAGCAGAAGGACTTGGCTTT	GGAATATGTCCAGGAGGAGGATAGA
Tmem98	CCAAGATGAAGACGTCAGCAAGTGTCAGTG	CAGAAAAACTCGTTGCCATGAC	GTTTGGCCACCACAATGATG
Ctsc	TTCAACCCCTTCGAGCTGACAAATCATG	ACGATGACTTCCTACACTACCACAGT	CCATAGCCCACAAGCAAAACA
F2r	CTTTCTTGTGCCGTTGATCGTTTCCAC	CGTCCTCAGTGAGAACCTGATG	ACAAAGCCCGCGACTTCTT
Sema3e	CCGAGCACAGCAGTAAAGGTAGAAGAATGC	GTGAGTGACGGCTACAGAGAGATATACT	CACACTCATTTGCGTCTTTTCC
Maged2	AGGCTATGACAATGCCTACAACCCCGA	AGCTGACACCAAGACGCAGAA	GTACCCTCAGGCTCTGGTTCAT
2810405K02Rik	TGTCTGGTGACCTGCTGCAAAGTGGA	CCAAGGCTAAAGCTGTTGGTATC	TCTGGATGAAGTGCAACAGTACCT
Rhox4b	TGTGGGCGTGAATGGAAAGTCTA	GCCCTAATTATTCTTGTCCTTATTTGTAA	CGCAGGCTTCCTACCTTGTG
Cd302	ACCTGTGGTTTTCTGTACACCAAGAC	GATCAAGATGGTGAGGACCTAGTTG	CACAATCCCCTTTTCTCCATTC
Fzd1	ACTTCTTTCCTGCTGGCCGGTTTCGT	CGCCTCTCTTCGTTTATCTGTTC	TCTCTGTCTTGGTGCCGTCAT
Adarb1	ACCTGCCACCGCTCTACACTCTCAACAA	GTACCAGCGGATCTCCAACATAG	TGCCTCTGCATTGCTGATG
Gpaa1	CAGCGCACTTACATGTCTGAGAATGCCA	TGGCTTTTCCGCCGTTAAC	CAAACTGTTCTCTCACCATGGT
Chst2	CTTCGGTGAGCTCTTCAACCAGAAC	GACAAGCGGCAGTTGGTGTAT	CCACACAGGCTCATAGAGGAAGA
9830115L13Rik	TCCACCAGGACATTAGACAGTCGTAAAG	AGGTTGTAGGTCCCGCATACA	CCACACACAAACTGTTCGTTCTG
9630055N22Rik	CAGATGGTTTCAGAAGCTGTTGCA	CATCACCTGTGTCTGCCTTCA	GGTGGCATTCCAGTTGCTAAC
Ptprb	TGCATGCACGGTTTAGAGCAGAAGTCG	GAACAGTTCACGGCTCCACATACC	ATCCAAAGCACACAGCCAGAA
Gstz1	AGGCATTGACTATGAGATAGTGCCCA	TCGAATTGCTCTGGCGTTAA	GTTGCCCGCCATCCTTTAT
1110021L09Rik	CAGAAAGCTGGCTCACCAAGGCAACA	CTGGAAGTGTCAAGCTGCATTT	TGGCTGGTTTGCCCTTTCT
Tsga14	AAGTGACAGCTGAGGAGATCCAAAGGCTC	CAAGTCGCTTCCCTGTCAGAT	CTCCCGTGCTGTTGATGAACT
Hnrnpa1	TTCTCAGCGACCAGGTGCCCACTTAACT	GTTGTGGAACCTAAGAGAGCTGTCT	CGTAGGTGATGTTCTTCAGTGTCTTC
Adm	TACAAGCCAGCAATCAGAGCGAAGC	CTCGCTGATGAGACGACAGTTC	GGTAGCGTTTGACACGAATGTG

Table S2 Oligonucleotide sequences for siRNAs targeting CMR genes

Gene names are provided in the main paper.

CMR gene number	Target gene	Sense sequences (5′→3′)	Antisense sequences (5′→3′)
1	*Prdm5*	GGGACAGUUGGCAGCUGGAAGUAAA	UUUACUUCCAGCUGCCAACUGUCCC
2	*AW551984*	CCGGUGAAGUGUGUCUCUCAUAUAA	UUAUAUGAGAGACACACUUCACCGG
3	*D430028G21Rik*	GCUGAGGACAAGACCUAUAAGUAUA	UAUACUUAUAGGUCUUGUCCUCAGC
4	*5330410G16Rik*	CCGGGCUGCCUCGAUGGGUCCUAUU	AAUAGGACCCAUCGAGGCAGCCCGG
5	*Tmem98*	CCACUGCAUCGCCAUCUUGAAGAUU	AAUCUUCAAGAUGGCGAUGCAGUGG
6	*Ctsc*	CCAAGGCUUCGAGAUUGUGUUGAAU	AUUCAACACAAUCUCGAAGCCUUGG
7	*F2r*	GGUAGGGCAGUCUACUUAAAUAUAA	UUAUAUUUAAGUAGACUGCCCUACC
8	*Sema3e*	CCAUACAAUGCUGCUGGAUGAGUAU	AUACUCAUCCAGCAGCAUUGUAUGG
9	*Maged2*	GGUACCGAUCCAAAGGUCAAUACAA	UUGUAUUGACCUUUGGAUCGGUACC
10	*2810405K02Rik*	GCCUCCAAGGCUAAAGCUGUUGGUA	UACCAACAGCUUUAGCCUUGGAGGC
11	*Rhox4b*	AAGCGGACGCCGTGGTCAAGA	UCUUGACCACGGCGUCCGCUU
12	*Cd302*	GGCAGACAUGGUAAGCAUACACAAU	AUUGUGUAUGCUUACCAUGUCUGCC
13	*Fzd1*	CCAAGGUUUACGGGCUCAUGUACUU	AAGUACAUGAGCCCGUAAACCUUGG
14	*Adarb1*	GGGACGAAGUGUAUCAACGGUGAAU	AUUCACCGUUGAUACACUUCGUCCC
15	*Gpaa1*	CCCAGCGCACUUACAUGUCUGAGAA	UUCUCAGACAUGUAAGUGCGCUGGG
16	*Chst2*	GGUGAGUCCCGAAAUGGAGCAGUUU	AAACUGCUCCAUUUCGGGACUCACC
17	*9830115L13Rik*	CCCUUGCUCCGUUACCUAACGACUU	AAGUCGUUAGGUAACGGAGCAAGGG
18	*9630055N22Rik*	CCUUGAAAUACUAGCUGCUGUCUUU	AAAGACAGCAGCUAGUAUUUCAAGG
19	*Ptprb*	GCAACUGAACCUGUUAUGUUCUAUA	UAUAGAACAUAACAGGUUCAGUUGC
20	*Gstz1*	GGGAAGCCUAUCCUCUACUCCUAUU	AAUAGGAGUAGAGGAUAGGCUUCCC
21	*1110021L09Rik*	CCCAGUCCAGAGCAUUUCUUGGCUU	AAGCCAAGAAAUGCUCUGGACUGGG
22	*Tsga14*	CCCAUUGCAACUCUAUCCAGGACAA	UUGUCCUGGAUAGAGUUGCAAUGGG
23	*Hnrnpa1*	GGAACACUAACAGACUGUGUGGUAA	UUACCACACAGUCUGUUAGUGUUCC
24	*Adm*	GCUGGUUUCCAUCACCCUGAUGUUA	UAACAUCAGGGUGAUGGAAACCAGC

Table S3 Correlation of GeneChip probe set intensities with the first and second principal components, lag time to the onset of beating and number of nodules

rs, Spearman's rank correlation coefficient.

CMR gene number	First principal component		Second principal component		Lag time to the onset of beating		Number of nodules	
	rs	*P* value	rs	*P* value	rs	*P* value	rs	*P* value
CMR1	0.8237	2.26×10^{-8}	0.7368	3.44×10^{-6}	−0.4932	5.61×10^{-3}	0.4384	1.54×10^{-2}
CMR2	0.7836	3.04×10^{-7}	0.7464	2.18×10^{-6}	−0.5419	1.98×10^{-3}	0.4153	2.25×10^{-2}
CMR3	0.7596	1.13×10^{-6}	0.4397	1.51×10^{-2}	−0.6333	1.73×10^{-4}	0.6455	1.17×10^{-4}
CMR4	0.7596	1.13×10^{-6}	0.6386	1.46×10^{-4}	−0.4859	6.48×10^{-3}	0.4202	2.08×10^{-2}
CMR5	0.7573	1.27×10^{-6}	0.466	9.44×10^{-3}	−0.6856	2.90×10^{-5}	0.6881	2.64×10^{-5}
CMR6	−0.7196	7.42×10^{-6}	−0.5235	2.99×10^{-3}	0.6771	3.97×10^{-5}	−0.5907	5.90×10^{-4}
CMR7	0.6589	7.52×10^{-5}	0.1282	5.00×10^{-1}	−0.492	5.75×10^{-3}	0.6004	4.52×10^{-4}
CMR2	0.6521	9.46×10^{-5}	0.3798	3.85×10^{-2}	−0.8038	8.85×10^{-8}	0.7672	7.57×10^{-7}
CMR8	−0.6246	2.25×10^{-4}	−0.4588	1.08×10^{-2}	0.4177	2.16×10^{-2}	−0.3824	3.70×10^{-2}
CMR9	−0.5903	5.96×10^{-4}	−0.3103	9.52×10^{-2}	0.503	4.61×10^{-3}	−0.5164	3.49×10^{-3}
CMR10	0.5658	1.12×10^{-3}	0.2336	2.14×10^{-1}	−0.6151	2.98×10^{-4}	0.6455	1.17×10^{-4}
CMR11	0.5651	1.14×10^{-3}	0.4277	1.84×10^{-2}	−0.6308	1.86×10^{-4}	0.5858	6.71×10^{-4}
CMR12	0.556	1.42×10^{-3}	0.4157	2.23×10^{-2}	−0.3982	2.93×10^{-2}	0.4165	2.21×10^{-2}
CMR13	0.5399	2.07×10^{-3}	0.3055	1.01×10^{-1}	−0.4299	1.77×10^{-2}	0.4323	1.70×10^{-2}
CMR13	0.5388	2.13×10^{-3}	0.1761	3.52×10^{-1}	−0.5858	6.71×10^{-4}	0.682	3.32×10^{-5}
CMR14	0.5366	2.24×10^{-3}	0.2432	1.95×10^{-1}	−0.4671	9.26×10^{-3}	0.5012	4.78×10^{-3}
CMR15	0.485	6.59×10^{-3}	0.0012	9.95×10^{-1}	−0.6735	4.53×10^{-5}	0.7806	3.61×10^{-7}
CMR16	0.4685	9.02×10^{-3}	−0.1186	5.32×10^{-1}	−0.4744	8.08×10^{-3}	0.64	1.40×10^{-4}
CMR17	−0.4559	1.13×10^{-2}	−0.0503	7.92×10^{-1}	0.7673	7.53×10^{-7}	−0.8313	1.28×10^{-8}
CMR18	0.453	1.19×10^{-2}	−0.0635	7.39×10^{-1}	−0.369	4.48×10^{-2}	0.548	1.72×10^{-3}
CMR19	−0.4404	1.49×10^{-2}	−0.1066	5.75×10^{-1}	0.643	1.27×10^{-4}	−0.7124	1.00×10^{-5}
CMR20	−0.4256	1.91×10^{-2}	0.0036	9.85×10^{-1}	0.4214	2.04×10^{-2}	−0.5395	2.09×10^{-3}
CMR21	0.397	2.99×10^{-2}	−0.0204	9.15×10^{-1}	−0.5809	7.63×10^{-4}	0.6832	3.17×10^{-5}
CMR22	−0.3924	3.20×10^{-2}	−0.2839	1.28×10^{-1}	0.5249	2.90×10^{-3}	−0.4579	1.09×10^{-2}
CMR23	−0.3924	3.20×10^{-2}	0.109	5.66×10^{-1}	0.6978	1.81×10^{-5}	−0.822	2.54×10^{-8}
CMR24	−0.3856	3.53×10^{-2}	0.1414	4.56×10^{-1}	0.4623	1.01×10^{-2}	−0.603	4.20×10^{-4}

Table S4 Effects of CMR gene knockdown on cardiac marker gene expression and the number of nodules in differentiated EC cells and ES cells

*Not significant (NS; $P \geqslant 0.05$); †transcript expression significantly decreased compared with the control ($P < 0.05$); ‡transcript expression significantly increased compared with the control ($P < 0.05$).

	Myh6 (α-MHC)		*Myh7* (β-MHC)		*Mlc2a*		*Mlc2v*		
Gene targeted	EC cells	ES cells	EC cells	ES cells	EC cells	ES cells	EC cells	ES cells	Number of nodules (EC cells)
CMR1	NS*	NS	NS	NS	NS	NS	NS	NS	NS
CMR2	Down†	Down	Down	Down	Down	Down	Down	Down	Down
CMR3	Down	NS	NS	NS	NS	NS	Down	NS	Down
CMR4	Down	NS	NS	NS	Down	NS	Down	NS	Down
CNR5	Down	NS	NS	NS	NS	NS	Down	NS	Down
CMR6	NS	NS	NS	NS	NS	NS	Down	NS	NS
CMR7	NS	NS	NS	Up‡	NS	Up	Up	NS	Up
CMR8	NS	Down	NS	Down	Down	Down	NS	NS	NS
CMR9	NS	NS	NS	Up	NS	Up	NS	Up	Down
CMR10	Down	Down	NS	Down	Down	Down	Down	Down	Down
CMR12	Up	Up	NS	Up	NS	Up	Up	NS	Up
CMR13	Down	NS	Down	NS	NS	NS	Down	NS	Down
CMR14	NS	Down	NS	Down	NS	Down	NS	Down	NS
CMR15	NS	Down	NS	Down	NS	Down	NS	Down	NS
CMR16	NS	NS	Up	NS	Up	NS	Up	NS	Up
CMR17	NS	NS	Up	NS	NS	NS	NS	NS	Up
CMR18	Down	NS	NS	NS	NS	NS	NS	NS	Down
CMR20	NS	Down	NS	NS	Down	Down	NS	NS	NS
CMR21	NS	NS	NS	Up	NS	Up	NS	NS	Up
CMR23	Up	Down	Up	Down	Down	Down	Up	Down	Up
CMR24	NS	NS	NS	Up	NS	Up	NS	NS	Down

Received 22 March 2011/3 May 2011; accepted 10 May 2011
Published as BJ Immediate Publication 10 May 2011, doi:10.1042/BJ20110520

Biochemical and Biophysical Research Communications 409 (2011) 108–113

Contents lists available at ScienceDirect

Biochemical and Biophysical Research Communications

journal homepage: www.elsevier.com/locate/ybbrc

TRPC3-mediated Ca^{2+} influx contributes to Rac1-mediated production of reactive oxygen species in MLP-deficient mouse hearts

Naoyuki Kitajima [a], Kunihiro Watanabe [a], Sachio Morimoto [b], Yoji Sato [c], Shigeki Kiyonaka [d], Masahiko Hoshijima [e], Yasuhiro Ikeda [f], Michio Nakaya [a], Tomomi Ide [g], Yasuo Mori [d], Hitoshi Kurose [a], Motohiro Nishida [a,*]

[a] Department of Pharmacology and Toxicology, Graduate School of Pharmaceutical Sciences, Kyushu University, Fukuoka 812-8582, Japan
[b] Department of Clinical Pharmacology, Graduate School of Medical Sciences, Kyushu University, Fukuoka 812-8582, Japan
[c] Division of Cellular and Gene Therapy Products, National Institute of Health Sciences, Tokyo 158-8501, Japan
[d] Laboratory of Molecular Biology, Department of Synthetic Chemistry and Biological Chemistry, Graduate School of Engineering, Kyoto University, Kyoto 615-8510, Japan
[e] Department of Medicine, Division of Cardiology, University of California San Diego, La Jolla, CA 92093-0734, USA
[f] Division of Cardiology, Department of Medicine and Clinical Science, Yamaguchi University Graduate School of Medicine, Yamaguchi 755-8505, Japan
[g] Department of Cardiovascular Medicine, Graduate School of Medical Sciences, Kyushu University, Fukuoka 812-8582, Japan

ARTICLE INFO

Article history:
Received 19 April 2011
Available online 3 May 2011

Keywords:
Transient receptor potential channel
Muscle LIM protein
Dilated cardiomyopathy
Rac
Reactive oxygen species

ABSTRACT

Dilated cardiomyopathy (DCM) is a myocardial disorder that is characterized by dilation and dysfunction of the left ventricle (LV). Accumulating evidence has implicated aberrant Ca^{2+} signaling and oxidative stress in the progression of DCM, but the molecular details are unknown. In the present study, we report that inhibition of the transient receptor potential canonical 3 (TRPC3) channels partially prevents LV dilation and dysfunction in muscle LIM protein-deficient (MLP (−/−)) mice, a murine model of DCM. The expression level of TRPC3 and the activity of Ca^{2+}/calmodulin-dependent kinase II (CaMKII) were increased in MLP (−/−) mouse hearts. Acitivity of Rac1, a small GTP-binding protein that participates in NADPH oxidase (Nox) activation, and the production of reactive oxygen species (ROS) were also increased in MLP (−/−) mouse hearts. Treatment with pyrazole-3, a TRPC3 selective inhibitor, strongly suppressed the increased activities of CaMKII and Rac1, as well as ROS production. In contrast, activation of TRPC3 by 1-oleoyl-2-acetyl-*sn*-glycerol (OAG), or by mechanical stretch, induced ROS production in rat neonatal cardiomyocytes. These results suggest that up-regulation of TRPC3 is responsible for the increase in CaMKII activity and the Nox-mediated ROS production in MLP (−/−) mouse cardiomyocytes, and that inhibition of TRPC3 is an effective therapeutic strategy to prevent the progression of DCM.

1. Introduction

Dilated cardiomyopathy (DCM), a poorly understood disorder in which the LV chambers enlarge, is the most common causes for congestive heart failure [1]. Heart failure resulting from DCM is a principal cause of death and disability in children and young adults. Despite recent progress in the treatment of heart failure, the only meaningful treatment for DCM is cardiac transplantation. Although most cases of DCM develop as a consequence of specific inflammatory, metabolic or toxic insults [2], 25–35% of DCM cases are caused by genetic mutations [3–5]. Affected genes encode proteins that function in the Ca^{2+} regulatory system, the contractile/cytoskeltal apparatus, or reside at a sarcomeric Z-disk. One of the Z-disk proteins that has been implicated in DCM etiology is the muscle LIM protein (MLP) [6–8]. MLP interacts with telethonin, a titin-interacting protein, to form a component of the mechanical stretch apparatus [8], and genetic ablation of MLP in mice causes age-related DCM, which closely resembles human DCM [8,9]. Thus, MLP deficient (MLP (−/−)) mice are commonly employed as a murine DCM model system. Since genetic ablation of angiotensin (Ang) II type1 receptor (AT_1R) or overexpression of the carboxyl-terminal region of the β adrenergic receptor (βAR) kinase (βARK-ct) attenuates the

Abbreviations: Ang, angiotensin; AT_1R, Ang type1 receptor; βAR, β adrenergic receptor; βARK, βAR kinase; βARK-ct, carboxyl-terminal region of βARK (βARK inhibitor); CaMKII, Ca^{2+}/calmodulin-dependent kinase II; DAG, diacylglycerol; DCF, dichlorofluorescein; DCM, dilated cardiomyopathy; DHE, dihydroethidium; DPI, diphenyleneiodonium; 4-HNE, 4-hydroxy-2-nonenal; LV, left ventricle; MLP, muscle LIM protein; LTCCs, L-type Ca^{2+} channels; NFAT, nuclear factor of activated T cells; Nox, NADPH oxidase; OAG, 1-oleoyl-2-acetyl-*sn*-glycerol; PKC, protein kinase C; pyrazole-3 (Pyr3), ethyl-1-(4-(2*3*3-trichloroacrylamide)phenyl)-5-(trifluoromethyl)-1H-pyrazole-4-carboxylate; ROS, reactive oxygen species; RIRR, ROS-induced ROS release; TRP, transient receptor potential; TRPC, TRP canonical.

* Corresponding author. Address: Department of Pharmacology and Toxicology, Graduate School of Pharmaceutical, Sciences, Kyushu University, 3-1-1 Maidashi, Higashi-ku, Fukuoka, Fukuoka 812-8582, Japan. Fax: +81 92 642 6878.
E-mail address: nishida@phar.kyushu-u.ac.jp (M. Nishida).

0006-291X/$ - see front matter © 2011 Elsevier Inc. All rights reserved.
doi:10.1016/j.bbrc.2011.04.124

progression of heart failure in MLP (−/−) mice [10,11], βAR and AT_1R signalings are thought to participate in the progression of heart failure in MLP (−/−) mice.

Abnormal Ca^{2+} metabolism and production of ROS have been implicated in the progressive deterioration of heart failure [12–14]. For example, activation of CaMKIIδ causes p53 accumulation and cardiomyocyte apoptosis in DCM [13]. In contrast, $p47^{phox}$, a Nox subunit, and the small GTP-binding protein Rac1, are up-regulated and oxygen free radical release is increased in human LV myocardium from patients with DCM [14]. Furthermore, oxidative stress inactivates calcineurin, a Ca^{2+}-dependent protein phosphatase that mediates cardiac hypertrophy, indicating the functional cross-talk between Ca^{2+} signaling and ROS signaling [12]. Although both Ca^{2+} and ROS evidently play key roles in the progression of heart failure, their upstream regulator(s) remain elusive.

Transient receptor potential (TRP) family proteins, first described in a *Drosophila* visual transduction mutation *trp*, comprise 28 mammalian cation channels expressed in almost every tissue [15–17]. Among them, canonical TRP subfamily (TRPC) proteins have been up-regulated in hypertrophied and failing hearts [17–20]. TRPC channels were originally proposed as store-operated channels activated by Ca^{2+} depletion of stores, while closely related TRPC3, TRPC6, and TRPC7 showed activation sensitivity to the membrane-delimited action of diacylglycerol (DAG). In particular, TRPC1, TRPC3 and TRPC6 proteins participate in agonist-induced cardiomyocyte hypertrophy through activation of Ca^{2+}-dependent calcineurin/nuclear factor of activated T cells (NFAT) signaling pathways [18–20]. We have reported that TRPC3 and TRPC6 channels mediate the Ang II-induced cardiomyocyte hypertrophy *in vitro* and pressure overload-induced cardiac hypertrophy *in vivo* [21,22]. The TRPC3/6-mediated cation influx induces membrane depolarization, followed by an increase in the frequency of Ca^{2+} transients evoked by voltage-dependent Ca^{2+} influx-induced Ca^{2+} release, leading to NFAT activation in rat cardiomyocytes [21]. However, calcineurin/NFAT signaling is apparently desensitized in MLP (−/−) mouse hearts, as MLP is essential for mechanical stretch-induced NFAT activation through anchorage of calcineurin at the Z-disk [23]. Therefore, it is unknown whether TRPC-mediated Ca^{2+} signals are involved in the progression of heart failure in MLP (−/−) mice.

In the present study, we examine the effects of a selective TRPC3 inhibitor, pyrazole-3 (Pyr3) [22], in the progression of DCM using the MLP (−/−) mouse model. We demonstrate that TRPC3-mediated Ca^{2+} signals are increased in MLP (−/−) mouse hearts, and Pyr3 potently inhibits LV dysfunction, CaMKII activation and ROS production. The inhibitory effect of Pyr3 on LV dysfunction is apparently small compared to the pronounced effects on CaMKII activation and ROS production, indicating that TRPC3 only plays a complementary role in the progression of DCM. However, our findings suggest that TRPC3 blockade is a therapeutic strategy for preventing DCM.

2. Materials and methods

2.1. Animals and drug treatment

The basal cardiomyopathic phenotype of MLP (−/−) mice was described previously [7,8]. Wild type littermates (MLP (+/+)) served as controls for all studies. A mini osmotic pump (Alzet) filled with pyrazole 3 (Pyr3), a selective inhibitor of TRPC3, or polyethylene glycol 300 (vehicle) was implanted intraperitoneally into 5-week-old mice, and Pyr3 (0.1 mg/kg/day) was continuously administered for 3 weeks. All animal care procedure and experiments were approved by the guidelines of Kyushu University.

2.2. Transthoracic echocardiography and cardiac catheterization

Echocardiography was performed in anesthetized mice (50 mg/kg pentobarbital sodium) by using Nemio-XG echocardiograph (TOSHIBA) equipped with a 14 MHz transducer. A 1.4 French micronanometer catheter (Millar Instruments, Houston, TX) was inserted into the left carotid and advanced retrograde into the LV. Hemodynamic measurements were recorded when heart rate was stabilized within 500 ± 10 beats/min.

2.3. Histological analysis of mouse hearts

The paraffin-embedded LV sections (5 μm in thickness) were stained with hematoxylin and eosin (H&E) or picrosirius red, and cell-sectional area (CSA) of cardiomyocytes and collagen volume fraction (CVF) of LV sections were analyzed using BZ-II analyzer (Keyence) [24].

2.4. Isolation of cardiomyocytes and siRNA treatment

Rat neonatal cardiomyocytes were prepared as described previously [25]. For knockdown of rat TRPC3 proteins, cells were transfected with siRNA (100 nM) for TRPC3 using lipofectamine2000 for 72 h [26]. Adult mouse cardiomyocytes were isolated from 8-week-old mouse hearts as described previously [5].

2.5. Real time PCR, pulldown assay, and Western blot analysis

RNA extraction, real time RT-PCR and Rac pulldown assay were performed as described previously [24]. Hearts were homogenized in RIPA buffer (pH 8.0) containing 0.1% SDS, 0.5% sodium deoxycholate, 1% NP-40, 150 mM NaCl, 50 mM Tris–HCl, and protease inhibitor cocktail (Nacalai). Supernatants (10 μg) were fractionated by SDS–PAGE gel, and expression levels of endogenous proteins were detected by antibodies raised against ACE (1/10,000, R&D systems), Periostin (1/10,000, R&D systems), Rac1 (1/1000, BD Bioscience), CaMKII (1/1000, Santa Cruz), phospho-CaMKII (Thr286) (1/1000, Cell Signaling) and GAPDH (1/3000, Santa Cruz). Membrane fractions (10 μg) were isolated using Proteoextract transmembrane protein extraction kit (Novagen) to detect TRPC1, TRPC3, TRPC5, TRPC6 and TRPC7 proteins using respective TRPC antibodies (1/2000, Alomone). Proteins were visualized with chemiluminescent detection of antibodies conjugated with horseradish peroxidase (ECL plus, Perkin Elmer). The optical density of the film was scanned and measured with Scion Image Software.

2.6. Measurement of ROS production and intracellular Ca^{2+} concentration

The paraffin-embedded LV sections were stained with anti-4-hydroxy-2-nonenal (4-HNE) antibody (1/500: JaICA, Nikken Seil Co., Ltd.). The 4-HNE adducts were visualized with Alexa Fluor 546 anti-mouse IgG antibody (1/1000, Molecular Probes). Superoxide production in the heart was measured using dihydroethidium (DHE) [27]. Hearts were solidified with liquid nitrogen and sectioned in 10 μm thickness using Cryostat (Leica, CM1100). The LV sections were incubated with DHE (100 μM) at room temperature for 5 min. After washing the LV sections with PBS, digital photographs were taken at ×60 magnification using confocal microscopy (FV10i, Olympus), and 5 regions selected at random for each specimen of the heart. The average intensity was analyzed using MetaMorph Software. Measurement of intracellular Ca^{2+} concentration ($[Ca^{2+}]_i$) in adult mouse cardiomyocytes was performed using fura-2 [26]. Production of ROS in rat neonatal cardiomyocytes was measured using 2′,7′-dichlorofluorescein diacetate ($DCFH_2DA$) and DHE [27]. Cells plated on laminin-coated silicone rubber

culture dishes were loaded with $DCFH_2DA$ (10 μM) at 37 °C for 10 min. The DCF fluorescence or fura-2 fluorescence at an emission wavelength of 510 nm was observed at room temperature by exciting DCF at 488 nm or exciting fura-2 at 340 nm and 380 nm using a video image analysis system (Aquacosmos, Hamamatsu Photonics).

2.7. Statistical analysis

The results are shown as means ± S.E.M. All experiments were repeated at least three times. Statistical comparisons were made with two-tailed Student's *t*-test or one way analysis of variance followed by the Student–Newman–Keuls procedure with significance imparted at $P < 0.05$.

3. Results

3.1. Increase in TRPC3-mediated Ca^{2+} signals in MLP (−/−) mouse hearts

Compared with MLP (+/+) mouse hearts, the expression levels of TRPC3 and TRPC6 proteins, but not TRPC1, TRPC5, and TRPC7, were significantly increased in MLP (−/−) mouse hearts (Fig. 1A). Treatment of isolated MLP (+/+) mouse cardiomyocytes with OAG induced a Ca^{2+} influx-mediated increase in $[Ca^{2+}]_i$. This $[Ca^{2+}]_i$ increase was completely suppressed by the addition of Pyr3 (Fig. 1B). The OAG-induced maximal $[Ca^{2+}]_i$ increase was markedly enhanced in MLP (−/−) mouse cardiomyocytes (Fig. 1C), indicating that up-regulation of TRPC3 enhances DAG-mediated Ca^{2+} influx. NFAT and CaMKII are two major downstream effectors of Ca^{2+}/calmodulin-mediated cardiac hypertrophy [17]. The CaMKII activity was increased in MLP (−/−) mouse hearts (Fig. 1D). This CaMKII activation was significantly suppressed by Pyr3 treatment. These results suggest that up-regulation of TRPC3 contributes to Ca^{2+} influx-dependent CaMKII activation in MLP (−/−) mouse hearts.

3.2. Inhibition of TRPC3 attenuates LV dilation and dysfunction

Both LV wall thickness and LV function were markedly reduced in 8-week-old MLP (−/−) mouse hearts (Tables 1 and 2). Treatment of MLP (−/−) mice with Pyr3 significantly attenuated the progression of LV dilation and dysfunction. Inhibition of TRPC3 also reduced the increase in heart weight and cardiomyocyte hypertrophy (Fig. 2A–C) and the increases in mRNAs of hypertrophy-related markers (β-myosin heavy chain (βMHC), α-skeletal muscle actin (αSKA) and Ang converting enzyme (ACE)) (Fig. 2D). We previously reported that cardiac hypertrophy and fibrosis are independently regulated by two heterotrimeric GTP-binding proteins [24]. Therefore, we next examined whether inhibition of TRPC3 suppresses cardiac fibrosis in MLP (−/−) mice. Collagen deposition in the interstitial area was markedly increased in MLP (−/−) hearts, and this fibrosis was suppressed by Pyr3 treatment (Fig. 3A and B). Pyr3 also suppressed the increase in expression of fibrosis-inducible proteins (ACE and periostin) in MLP (−/−) mouse hearts (Fig. 3C). These results suggest that inhibition of TRPC3 attenuates the development of cardiac hypertrophy and fibrosis in MLP (−/−) mice.

3.3. TRPC3-mediated Ca^{2+} influx contributes to ROS production

It is generally thought that oxygen free radical release is increased in the failing heart and oxidative stress is a major cause of the progression of heart failure [12,14]. Up-regulation of TRPC3 channels participate in CaMKII activation in MLP (−/−) mouse hearts, and it has been reported that Ca^{2+} influx is required for Nox-mediated ROS production [28,29]. Therefore, we examined whether TRPC3-mediated Ca^{2+} influx regulates ROS production in DCM. The expression level of 4-HNE adducts and superoxide production were markedly increased in MLP (−/−) mouse hearts (Fig. 4A and B). These ROS accumulations

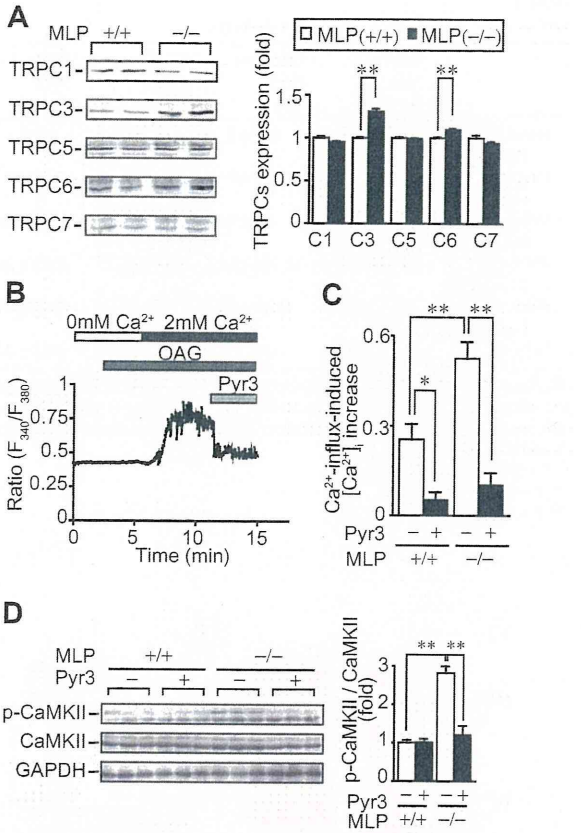

Fig. 1. Involvement of TRPC3 in CaMKII activation of MLP-deficient hearts. (A) Protein expression levels of respective TRPC channels in wild type (MLP (+/+)) and MLP-deficient (MLP (−/−)) mouse hearts. Hearts were removed from 5 week-old mice. ($n = 4$) $^{**}P < 0.01$ (B) Typical time course of Ca^{2+} response induced by OAG (15 μM) in the absence (0 mM Ca^{2+}) or presence of extracellular Ca^{2+} (2 mM Ca^{2+}) in isolated MLP (+/+) mouse cardiomyocytes. Cells were treated with Pyr3 (1 μM). ($n = 10$–12) (C) Maximal Ca^{2+} influx-mediated increase in $[Ca^{2+}]_i$ induced by OAG. (D) Effects of pyrazole-3 (Pyr3) on the phosphorylation of CaMKII proteins. ($n = 6$) $^{*}P < 0.05$.

Table 1
Echocardiographic parameters.

	MLP(+/+) Veh ($n = 5$)	MLP(+/+) Pyr3 ($n = 5$)	MLP(−/−) Veh ($n = 11$)	MLP(−/−) Pyr3 ($n = 11$)
HR (bpm)	538 ± 10	541 ± 14	533 ± 11	529 ± 16
IVSd (mm)	0.88 ± 0.04	0.90 ± 0.03	0.63 ± 0.03**	0.92 ± 0.04##
LVPWd (mm)	0.98 ± 0.02	0.94 ± 0.02	0.71 ± 0.04**	0.97 ± 0.04##
LVIDd (mm)	2.08 ± 0.09	2.04 ± 0.02	3.25 ± 0.17**	2.64 ± 0.04##
LVIDs (mm)	0.50 ± 0.06	0.48 ± 0.02	2.48 ± 0.19**	1.39 ± 0.18##
EF (%)	98.8 ± 0.3	98.8 ± 0.2	56.0 ± 3.9**	83.2 ± 3.4##
FS (%)	78.0 ± 2.1	78.0 ± 1.1	25.4 ± 1.1**	50.6 ± 4.7##

HR, heart rate; IVSd, interventricular septum diastolic diameter; LVPWd, left ventricular posterior wall diastolic diameter; LVIDd, left ventricular internal at end-diastole; LVIDs, left ventricular internal diameters at end-systole; EF, ejection fraction; FS, Fractional shortening; Veh, vehicle.
** $P < 0.01$ vs. MLP(+/+) Veh.
$P < 0.01$ vs. MLP(−/−) Veh.

Table 2
Cardiac parameters measured by Millar Catheter.

	MLP(+/+) Veh (n = 5)	MLP(+/+) Pyr3 (n = 5)	MLP(−/−) Veh (n = 11)	MLP(−/−) Pyr3 (n = 11)
Heart Rate (bpm)	498 ± 3	504 ± 2	500 ± 4	505 ± 1
LVESP (mm Hg)	123 ± 4	127 ± 3	102 ± 2**	108 ± 2#
LVEDP (mm Hg)	4.4 ± 0.8	3.6 ± 1.0	14.1 ± 1.2**	8.4 ± 0.4##**
dP/dt max (mm Hg/s)	13,365 ± 199	12,756 ± 412	6252 ± 294**	8235 ± 316##
dP/dt min (mm Hg/s)	8049 ± 617	8444 ± 530	3240 ± 185**	4516 ± 178##
Tau (msec)	9.8 ± 0.4	8.9 ± 0.2	28.7 ± 1.8**	20.2 ± 0.8##

HR, heart rate; LVESP, left ventricular end systolic pressure; LVEDP, left ventricular end diastolic pressure; dP/dt max, maximal rate of pressure development; dP/dt min, maximal rate of decay of pressure; Tau, monoexponential time constant of relaxation. Veh, vehicle.
** $P < 0.01$ vs. MLP(+/+) Veh.
# $P < 0.05$.
$P < 0.01$ vs. MLP(−/−) Veh.

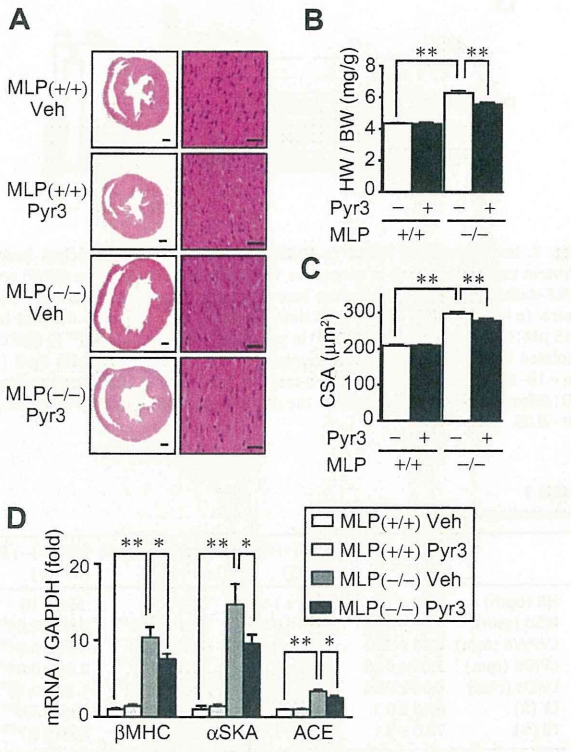

Fig. 2. Inhibition of TRPC3 attenuates left ventricular dysfunction in MLP-deficient mice. Effects of Pyr3 on morphological changes (A)–(C) and hypertrophic gene expression (D) in MLP (+/+) and MLP (−/−) mouse hearts. (A) H&E-stained mid-transverse LV sections of the hearts isolated from 8 week-old mice. Bars = 400 μm (left) and 50 μm (right). (n = 5–11) (B) Heart weight (HW) to body weight (BW) ratios. (C) Average areas of cardiomyocytes. (n = 5). (D) Expressions of β-MHC, α-SKA and ACE mRNAs. (n = 4) *$P < 0.05$, ** $P < 0.01$.

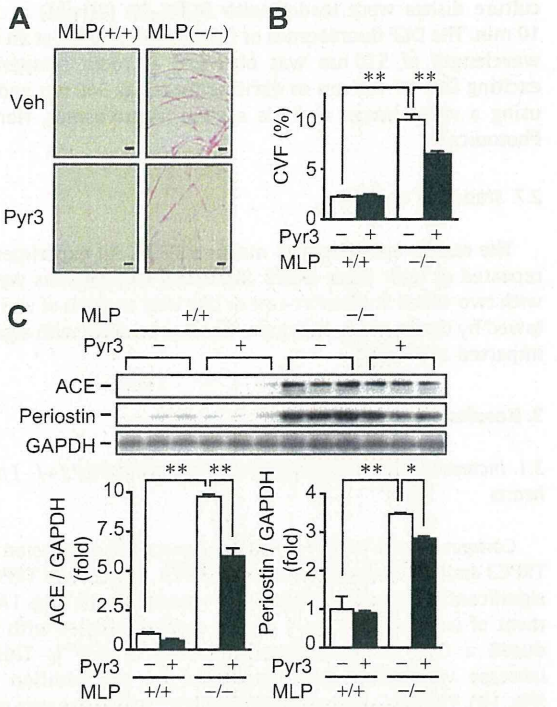

Fig. 3. Inhibition TRPC3 attenuates interstitial fibrosis of MLP-deficient mice. (A) LV sections stained by picrosirius red (Bars = 50 μm). (B) Results of fibrosis in MLP (−/−) and MLP (+/+) mouse hearts with or without Pyr3. (n = 5) (C) Effects of Pyr3 on the expressions of ACE, periostin, and GAPDH proteins. (n = 6) *$P < 0.05$, **$P < 0.01$.

were completely suppressed by Pyr3. Mitochondria and Nox are two major sources of ROS in the heart. The heart expresses two Nox isoforms: Nox2 and Nox4 [30,31], and up-regulation of either isoform has been reported to induce mitochondrial dysfunction in the heart [14,31]. The Nox2 activity is predominantly regulated by Rac, $p47^{phox}$, $p67^{phox}$, and $p22^{phox}$, while Nox4 is constitutively activated [32]. In addition, Rac1 has been implicated in the progression of DCM [14]. Although Nox2 and Nox4 mRNA levels were not increased in MLP (−/−) mouse hearts (data not shown), the expression and activity of Rac1 were markedly increased (Fig. 4C). Treatment with Pyr3 significantly suppressed Rac1 activation without affecting total Rac1 protein levels. These results suggest that up-regulation of TRPC3 contributes to Rac1-mediated ROS production in MLP (−/−) mouse hearts. We further examined whether activation of TRPC3 actually induces ROS production in rat neonatal cardiomyocytes. We recently reported that mechanical stretch induces a Ca^{2+} response through activation of TRPC3/6 channels [26]. Mechanical stretch of cardiomyocytes gradually increased DCF fluorescence intensity (Fig. 4D). This ROS production was significantly suppressed by Pyr3 or knockdown of TRPC3. Treatment with OAG also induced superoxide production, and the DHE accumulation was reduced by TRPC3 knockdown or by pretreatment with Pyr3 or diphenyleneiodonium (DPI), a Nox inhibitor (Fig. 4E and F). Furthermore, the OAG-induced superoxide production was inhibited by the elimination of extracellular Ca^{2+}. These results suggest that TRPC3-mediated Ca^{2+} influx mediates ROS production through Nox activation in rodent cardiomyocytes.

4. Discussion

Several reports have suggested the involvement of TRPC up-regulation in the development of cardiac hypertrophy *in vivo* [17–20]. On the other hand, DCM is believed to represent a maladaptive response of the heart in a late stage of heart failure. We first demonstrated that TRPC3 channels participate in the

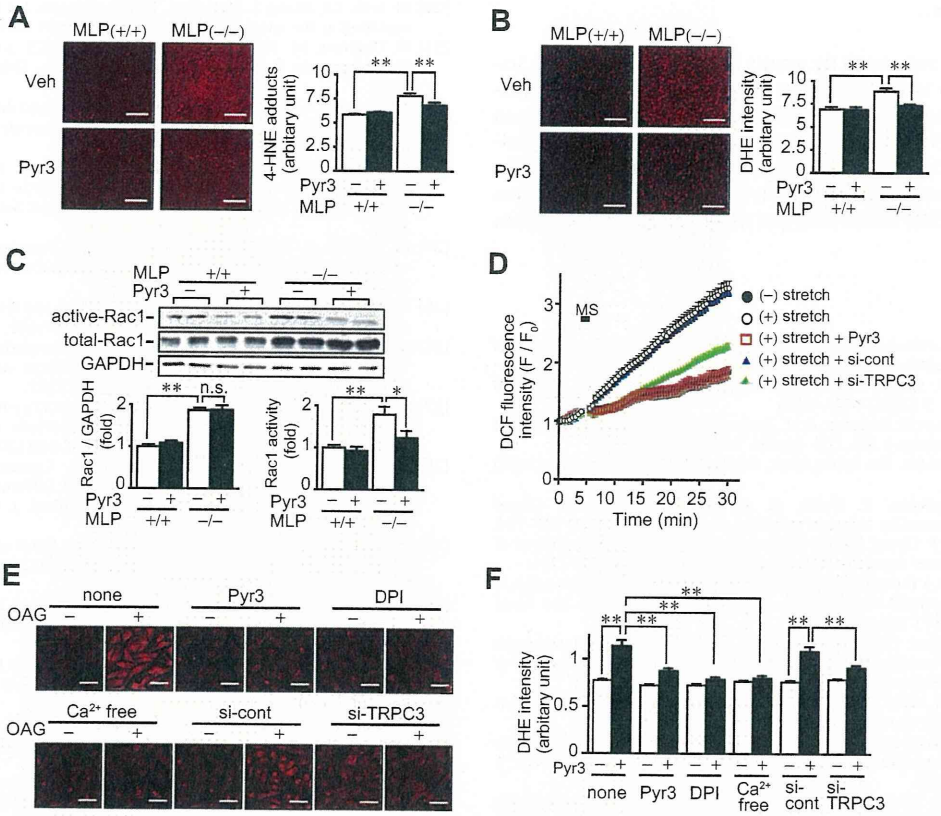

Fig. 4. TRPC3 mediates mechanical stretch-induced superoxide production in cardiomyocytes. (A) Immunostaining for 4-HNE adducts of the hearts. (B) Superoxide production of the hearts stained by DHE. Bars = 50 μm. ($n = 5$) (C) Effects of Pyr3 on the expression and activity of Rac1 in MLP (−/−) and MLP (+/+) mouse hearts. n.s.; not significant. ($n = 6$) (D) Average time courses of increase in DCF fluorescence intensity induced by mechanical stretch in rat neonatal cardiomyocytes. Cardiomyocytes were treated with Pyr3 (1 μM) 30 min before mechanical stretch. (E) and (F) Effects of Pyr3 on the OAG-induced ROS production in rat cardiomyocytes. (E) Typical images of DHE accumulation and (F) average increases in DHE fluorescence intensity. Cells were treated with Pyr3 (1 μM) or DPI (1 μM) for 20 min before the addition of OAG (30 μM). Ten min after OAG stimulation, cells were loaded with DHE (2 μM) at 37 °C for 1 h. Bars = 50 μm. ($n = 34$–63) $^{*}P < 0.01$, $^{**}P < 0.001$.

progression of DCM. In the DCM mouse model, the up-regulation of TRPC3 increases not only cardiomyocyte Ca^{2+}-dependent CaMKII activity, but also ROS production. TRPC channels have two functions: to act as receptor-activated or mechanical stretch-activated cation channels in cardiomyocytes, and to act as a protein scaffold at the plasma membrane to control the amplification and co-ordination of receptor signaling [16,33,34]. We previously reported that TRPC3 interacts with phospholipase C and protein kinase C (PKC), leading to sustained activation of an extracellular signal-regulated kinase induced by receptor stimulation in B lymphocytes [33,34]. Activation of PKC contributes to Nox2 activation through phosphorylation of the $p47^{phox}$ subunit [32]. In addition, we found that TRPC3-mediated Ca^{2+} influx also contributes to Rac1 activation in MLP (−/−) mouse hearts (Fig. 4). Although the molecular mechanism underlying activation of Rac1 by Ca^{2+} is still unclear, our results strongly suggest that TRPC3-mediated Ca^{2+} influx controls Nox-dependent ROS production in rodent cardiomyocytes.

Oxidative stress plays a critical role in the progression of DCM, and the major source of ROS production in the heart is mitochondria. Based on the results that the increase in ROS production was associated with an increase in Rac activity in MLP (−/−) mouse hearts, and that the Nox inhibitor suppressed TRPC3-mediated superoxide production in rat cardiomyocytes (Fig. 4), Nox may be a primary source of ROS production. ROS have been reported to induce mitochondrial superoxide production, by a phenomenon reported as ROS-induced ROS release (RIRR) [35,36]. Thus, TRPC3-mediated Ca^{2+} influx in rodent cardiomyocytes may initially induce Nox-dependent ROS production, with the subsequent induction of an oxygen burst through RIRR-mediated ROS production.

Previous reports have shown that ablation of AT_1R or expression of βARK-ct attenuates LV dysfunction in MLP (−/−) mice. We also reported that TRPC3/TRPC6 mediates Ang II-induced cardiomyocyte hypertrophy [21], suggesting that AT_1R works upstream of TRPC3 in MLP (−/−) mouse hearts. In contrast, βARK-ct inhibits βARK1-mediated β_1AR internalization through sequestration of the βγ subunit (Gβγ) released from the α_s subunit of G proteins coupled to β_1AR. However, inhibition of TRPC3 does not affect β_1AR-mediated Ca^{2+} signaling in rat cardiomyocytes (unpublished data). As βARK is activated by Gαq-mediated PKC activation in rat cardiomyocytes [37], one explanation is that TRPC3 contributes to PKC-mediated βARK activation downstream of AT_1R signaling in the heart [34].

Both Ca^{2+}/calmodulin-dependent calcineurin and CaMKII function as key mediators in the development of cardiac hypertrophy [38,39]. Cardiomyocyte-specific overexpression of the constitutively active mutant of NFAT causes cardiac hypertrophy, whereas expression of calcineurin or CaMKII causes cardiomyopathy [13,40]. Although calcineurin/NFAT signaling may participate in the development of hypertrophy, CaMKII may participate in the development of heart failure. Since the inhibition of TRPC3 suppresses both calcineurin/NFAT and CaMKII signaling pathways in cardiomyocytes, our findings strongly suggest TRPC3 channels as a putative therapeutic target for the treatment of heart failure.

Acknowledgments

This study was supported by grants from Grant-in-Aid for Scientific Research on Innovative Areas (M. Nishida); from the Ministry of Education, Culture, Sports, Science, and Technology of Japan (to M. Nishida, M. Nakaya and H. Kurose); from the Institute of Seizon and Life Sciences (to S. Morimoto) and from Naito Foundation and Mochida Memorial Foundation (M. Nishida). M. Hoshijima was supported by NIH (R01 HL081401) and American Heart Association (0840013N).

References

[1] J.A. Towbin, A.M. Lowe, S.D. Colan, et al., Incidence, causes, and outcomes of dilated cardiomyopathy in children, JAMA 296 (2006) 1867–1876.
[2] W.B. Maclellan, A. Lusis, Dilated cardiomyopathy: learning to live with yourself, Nat. Med. 9 (2003) 1455–1456.
[3] E. Grunig, J.A. Tasman, H. Kucherer, et al., Frequency and phenotypes of familial dilated cardiomyopathy, J. Am. Coll. Cardiol. 31 (1998) 186–194.
[4] J.A. Towbin, N.E. Bowles, The failing heart, Nat. Insight rev. articles 415 (2002) 227–233.
[5] C.-K. Du, S. Morimoto, K. Nishii, et al., Knock-in model of dilated cardiomyopathy caused by troponin mutation, Circ. Res. 101 (2007) 185–194.
[6] S. Arber, G. Halder, P. Caroni, Muscle LIM protein, a novel essential regulator of myogenesis, promotes myogenic differentiation, Cell 79 (1994) 221–231.
[7] S. Arber, J.J. Hunter, J. Ross Jr, et al., MLP-deficient mice exhibit a disruption of cardiac cytoarchitectural organization, dilated cardiomyopathy, and heart failure, Cell 88 (1997) 393–403.
[8] R. Knöll, M. Hoshijima, H.M. Hoffman, et al., The cardiac mechanical stretch sensor machinery involves a Z-disc complex that is defective in a subset of human dilated cardiomyopathy, Cell 111 (2002) 943–955.
[9] R. Knöll, S. Kostin, S. Klede, et al., A common MLP (muscle LIM protein) variant is associated with cardiomyopathy, Circ. Res. 106 (2010) 695–704.
[10] R. Yamamoto, H. Akazawa, K. Ito, et al., Angiotensin II type 1a receptor signals are involved in the progression of heart failure in MLP-deficient mice, Circ. J. 71 (2007) 1958–1964.
[11] H.A. Rockman, K.R. Chien, D.-J. Choi, et al., Expression of a β-adrenergic receptor kinase 1 inhibitor prevents the development of myocardial failure in gene-targeted mice, Proc. Natl. Acad. Sci. USA 95 (1998) 7000–7005.
[12] X. Wang, V.C. Culotta, C.B. Klee, Superoxide dismutase protects calcineurin from inactivation, Nature 383 (1996) 434–437.
[13] H. Toko, H. Takahashi, Y. Kayama, et al., Ca^{2+}/calmodulin-dependent kinase IIδ causes heart failure by accumulation of p53 in dilated cardiomyopathy, Circulation 122 (2010) 891–899.
[14] C. Maack, T. Kartes, H. Kilter, et al., Oxygen free radical release in human failing myocardium is associated with increased activity of Rac1-GTPase and represents a target for statin treatment, Circulation 108 (2003) 1567–1574.
[15] C. Montell, G.M. Rubin, Molecular characterization of the Drosophila trp locus: a putative integral membrane protein required for phototransduction, Neuron 2 (1989) 1313–1323.
[16] M. Nishida, Y. Hara, T. Yoshida, et al., TRP channels: molecular diversity and physiological function, Microcirculation 13 (2006) 535–550.
[17] M. Nishida, H. Kurose, Roles of TRP channels in the development of cardiac hypertrophy, Naunyn–Schmiedeberg's Arch. Pharmacol. 378 (2008) 395–406.
[18] E.W. Bush, D.B. Hood, P.J. Papst, et al., Canonical transient receptor potential channels promote cardiomyocyte hypertrophy through activation of calcineurin signaling, J. Biol. Chem. 281 (2006) 33487–33496.
[19] K. Kuwahara, Y. Wang, J. McAnally, et al., TRPC6 fulfills a calcineurin signaling circuit during pathologic cardiac remodeling, J. Clin. Invest. 116 (2006) 3114–3126.
[20] M. Seth, Z.S. Zhang, L. Mao, et al., TRPC1 channels are critical for hypertrophic signaling in the heart, Circ. Res. 105 (2009) 1023–1030.
[21] N. Onohara, M. Nishida, R. Inoue, et al., TRPC3 and TRPC6 are essential for angiotensin II-induced cardiac hypertrophy, EMBO J. 25 (2006) 5305–5316.
[22] S. Kiyonaka, K. Kato, M. Nishida, et al., Selective and direct inhibition of TRPC3 channels underlies biological activities of a pyrazole compound, Proc. Natl. Acad. Sci. USA 106 (2009) 5400–5405.
[23] J. Heineke, H. Ruetten, C. Willenbockel, et al., Attenuation of cardiac remodeling after myocardial infarction by muscle LIM protein-calcineurin signaling at the sarcomeric Z-disc, Proc. Natl. Acad. Sci. USA 102 (2005) 1655–1660.
[24] M. Nishida, Y. Sato, A. Uemura, et al., $P2Y_6$ receptor-$G\alpha 12_{/13}$ signalling in cardiomyocytes triggers pressure overload-induced cardiac fibrosis, EMBO J. 27 (2008) 3104–3115.
[25] M. Nishida, Y. Maruyama, R. Tanaka, et al., Gαi and Gαo are target proteins of reactive oxygen species, Nature 408 (2000) 492–495.
[26] M. Nishida, K. Watanabe, Y. Sato, et al., Phosphorylation of TRPC6 channels at Thr69 is required for anti-hypertrophic effects of phosphodiesterase 5 inhibition, J. Biol. Chem. 285 (2010) 13244–13253.
[27] T. Fujii, N. Onohara, Y. Maruyama, et al., $G\alpha 12_{/13}$-mediated production of reactive oxygen species is critical for angiotensin receptor-induced NFAT activation in cardiac fibroblasts, J. Biol. Chem. 280 (2005) 23041–23047.
[28] D. Granfeldt, M. Samuelsson, A. Karlsson, Capacitative Ca^{2+} influx and activation of the neutrophil respiratory burst. Different regulation of plasma membrane-and granule-localized NADPH-oxidase, J. Leukoc. Biol. 71 (2002) 611–617.
[29] D.B. Graham, C.M. Robertson, J. Bautista, et al., Neutrophil-mediated oxidative burst and host defense are controlled by a Vav-PLCγ2 signaling axis in mice, J. Clin. Invest. 117 (2007) 3445–3452.
[30] J.M. Li, N.P. Gall, D.J. Grieve, et al., Activation of NADPH oxidase during progression of cardiac hypertrophy to failure, Hypertension 40 (2002) 477–484.
[31] T. Ago, J. Kuroda, J. Pain, et al., Upregulation of Nox4 by hypertrophic stimuli promotes apoptosis and mitochondrial dysfunction in cardiac myocytes, Circ. Res. 106 (2010) 1253–1264.
[32] H. Sumimoto, Structure, regulation and evolution of Nox-family NADPH oxidases that produce reactive oxygen species, FEBS J. 275 (2008) 3249–3277.
[33] M. Nishida, K. Sugimoto, Y. Hara, et al., Amplification of receptor signaling by Ca^{2+} entry-mediated translocation and activation of PLCγ2 in B lymphocytes, EMBO J. 22 (2003) 4677–4688.
[34] T. Numaga, M. Nishida, S. Kiyonaka, et al., Ca^{2+} influx and protein scaffolding via TRPC3 sustain PKCβ and ERK activation in B cells, J. Cell. Sci. 123 (2010) 927–938.
[35] D.B. Zorov, C.R. Filburn, L.O. Klotz, et al., Reactive oxygen species (ROS)-induced ROS release: a new phenomenon accompanying induction of the mitochondrial permeability transition in cardiac myocytes, J. Exp. Med. 192 (2000) 1001–1014.
[36] N.R. Brady, A. Hamacher-Brady, H.V. Westerhoff, et al., A wave of reactive oxygen species (ROS)-induced ROS release in a sea of excitable mitochondria, Antioxid. Redox. Signal. 8 (2006) 1651–1665.
[37] R. Malhotra, K.M. D'Souza, M.L. Staron, et al., Gαq-mediated activation of GRK2 by mechanical stretch in cardiac myocytes: the role of protein kinase C, J. Biol. Chem. 285 (2010) 13748–13760.
[38] J.D. Molkentin, J.-R. Lu, C.L. Antos, et al., A calcineurin-dependent transcriptional pathway for cardiac hypertrophy, Cell 93 (1998) 215–228.
[39] R. Passier, H. Zeng, N. Frey, et al., CaM kinase signaling induces cardiac hypertrophy and activates the MEF2 transcription factor *in vivo*, J. Clin. Invest. 105 (2000) 1395–1406.
[40] M.R. Sayen, A.B. Gustafsson, M.A. Sussman, et al., Calcineurin transgenic mice have mitochondrial dysfunction and elevated superoxide production, Am. J. Physiol. Cell Physiol. 284 (2003) C562–570.

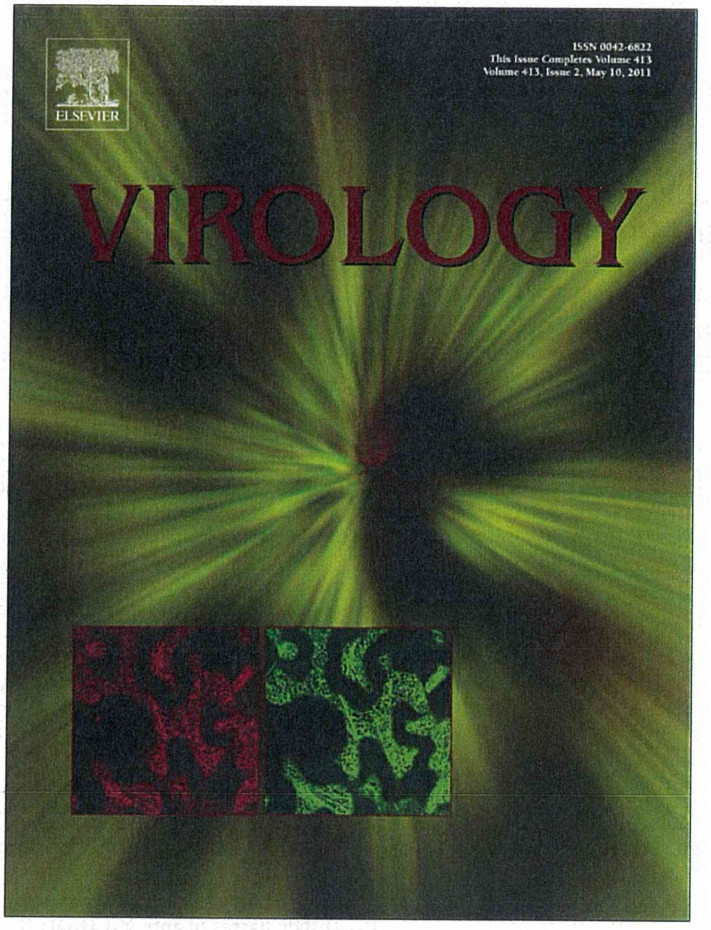

Virology 413 (2011) 293–299

Contents lists available at ScienceDirect

Virology

journal homepage: www.elsevier.com/locate/yviro

A combination of polymorphic mutations in V3 loop of HIV-1 gp120 can confer noncompetitive resistance to maraviroc

Yuzhe Yuan [a], Yosuke Maeda [a], Hiromi Terasawa [a], Kazuaki Monde [a], Shinji Harada [a], Keisuke Yusa [b,*]

[a] Department of Medical Virology, Graduate School of Medical Sciences, Kumamoto University, Honjo 1-1-1, Kumamoto 860–8665, Japan
[b] Division of Biological Chemistry and Biologicals, National Institute of Health Sciences Kami-youga 1-18-1, Setagaya, Tokyo 158–8501, Japan

ARTICLE INFO

Article history:
Received 21 December 2010
Returned to author for revision
14 January 2011
Accepted 24 February 2011
Available online 26 March 2011

Keywords:
HIV-1
CCR5
gp120
V3 loop
Viral entry
Maraviroc
Noncompetitive resistance

ABSTRACT

Maraviroc binds to the pocket of extracellular loops of the cell surface CCR5 and prevents R5 HIV-1 from using CCR5 as a coreceptor for entry into CD4-positive cells. To evaluate the contribution of the V3 loop structure in gp120 to maraviroc resistance, we isolated maraviroc-resistant variants from the V3 loop library virus (HIV-1_{V3Lib}) containing a set of random combinations of 0–10 polymorphic mutations *in vitro*. HIV-1_{V3Lib} at passage 17 could not be suppressed even at 10 μM (>1400-fold resistance), while HIV-$1_{JR\text{-}FL}$ at passage 17 revealed an 8-fold resistance to maraviroc. HIV-$1_{V3Lib\text{-}P17}$ contained T199K and T275M plus 5 mutations in the V3 loop, I304V/F312W/T314A/E317D/I318V. The profile of pseudotyped virus containing I304V/F312W/T314A/E317D/I318V in V3 loop alone revealed a typical noncompetitive resistance, although T199K and/or T275M could not confer noncompetitive resistance. This type of library virus is useful for isolation of escape viruses from effective entry inhibitors.

Introduction

The entry of human immunodeficiency virus type 1 (HIV-1) in target cells is a feasible step where small compounds could be used to block viral replication (Donzella et al., 1998; Dragic et al., 2000; Strizki et al., 2001; Trkola et al., 2002). To completely suppress viral entry *in vivo*, various antiviral agents have been developed that target unique viral proteins and receptors (Kuhmann and Hartley, 2008; Tsibris and Kuritzkes, 2007; Westby and van der Ryst, 2010). Enfuvirtide (Fuzeon) is an antiviral peptide that prevents HIV entry by blocking gp41-mediated fusion through interaction with the gp41 N-heptad repeat domain to form a heterologous trimer of heterodimer complex (Chan et al., 1997; Chan and Kim, 1998; Wild et al., 1993). Another target to block viral entry is CCR5. Small compounds that can bind to the pockets of the extracellular loops of CCR5 are expected to be potent antiviral agents. Several small-molecule CCR5 inhibitors have progressed through clinical development (Westby and van der Ryst, 2010). Maraviroc (Dorr et al., 2005; Fatkenheuer et al., 2005) is the first and only CCR5 antagonist approved by the U.S. Food and Drug Administration in 2007 for treatment-experienced patients with an R5-tropic virus.

The emergence of viruses resistant to entry inhibitors as well as other classes of antiviral agents has been reported *in vitro* and *in vivo* (Moore and Kuritzkes, 2009; Westby and van der Ryst, 2010). The intuitive manner of resistance to small-molecule CCR5 inhibitors depends on coreceptor switching from a CCR5-using virus to a dual-tropic virus or a CXCR4-using virus, but these are rare cases *in vitro* and *in vivo* (Maeda et al., 2008; Westby and van der Ryst, 2010). Virologic failure in clinical aspects is an outgrowth of the pre-existing minority population of the CXCR4-using virus (Gulick et al., 2007; Moore and Kuritzkes, 2009; Westby and van der Ryst, 2010). These results indicate that the acquisition of the other type of resistance occurs preferentially in R5 viruses because coreceptor switching requires multiple mutations throughout gp160 through transitional intermediates with poor replication fitness (Pastore et al., 2004). Two types of genetic pathways for virus escape have been reported *in vitro* (Marozsan et al., 2005; Pugach et al., 2007; Trkola et al., 2002). The first is the accumulation of multiple amino acid substitutions in Env including 2–4 substitutions in the gp120 V3 domain. Unique changes have been detected in different isolates (Baba et al., 2007; Kuhmann et al., 2004; Marozsan et al., 2005; Ogert et al., 2008; Pugach et al., 2007; Trkola et al., 2002; Westby et al., 2007). Some of these resistant viruses revealed noncompetitive resistance (Kuhmann et al., 2004; Trkola et al., 2002; Westby et al., 2007). In noncompetitive resistance, the escape variants could use the inhibitor-bound form of CCR5 as well as free CCR5 for entry. The second is a genetic pathway independent of V3 mutations. Resistance to vicriviroc has developed through multiple

* Corresponding author. Fax: +81 3 3700 9084.
E-mail address: yusak@nihs.go.jp (K. Yusa).

0042-6822/$ – see front matter © 2011 Elsevier Inc. All rights reserved.
doi:10.1016/j.virol.2011.02.019

amino acid substitutions throughout gp160 without any changes in the V3 loop (Marozsan et al., 2005). The determinants of resistance induced by vicriviroc have been mapped on a 200-residue stretch of gp120 spanning the C2–V5 region (Ogert et al., 2008). These reports indicate that resistance to small-molecule CCR5 inhibitors is complicated and there appears to be no common key mutations.

In this study, we used the V3 loop library virus (HIV-1_{V3Lib}), which carries a set of random combinations from 0 to 10 substitutions (27,648 possibilities) in the V3 loop (residues 302, 303, 304, 305, 306, 312, 314, 317, 318, and 321; V3 loop from Cys^{293} to Cys^{327}) (Yusa et al., 2005) (Fig. 1A). They were polymorphic mutations derived from 31 R5 clinical isolates. To further elucidate the contribution of the V3 loop to resistance to small-molecule CCR5 inhibitors, we selected maraviroc-resistant variants from HIV-1_{V3Lib}. We describe the isolation of maraviroc-resistant variants after 17 passages with a gradual increase in maraviroc concentration *in vitro*, and discuss the finding that the resistant variants from HIV-1_{V3Lib} revealed noncompetitive resistance to maraviroc.

Results

Selection of maraviroc-resistant variants from HIV-1_{JR-FL} and HIV-1_{V3Lib}

We used the replication-competent HIV-1_{V3Lib} for selection of maraviroc-resistant viruses. Each virus clone in the library contains a set of 0–10 amino acid substitutions in the gp120 V3 loop from Cys^{293} to Cys^{327} (Fig. 1A). We used PM1/CCR5 cells for virus passages because they have two advantages. First, PM1/CCR5 cells are highly sensitive to the R5 virus compared to the parental PM1 cells; second, prominent cell fusion caused by viral infection is a straightforward sign of virus proliferation. EC_{50}s of HIV-1_{JR-FL} and HIV-1_{V3Lib} to maraviroc were 0.0069 ± 0.0019 μM and 0.0055 ± 0.0007 μM, respectively (Table 1). The susceptibility of HIV-1_{V3Lib} to maraviroc was similar to that of the wild type. To select maraviroc-resistant variants, PM1/CCR5 cells were infected with HIV-1_{JR-FL} or HIV-1_{V3Lib} in the presence of 0.003 μM maraviroc in passage 1 (Fig. 1B). After infection, 4 to 7 days were required for the viruses to sufficiently replicate for the next passage. During the passages, the concentration of maraviroc was gradually increased up to 0.1 μM until passage 14 for HIV-1_{JR-FL} and HIV-1_{V3Lib} in the same manner. At passage 15, the library virus could replicate in 4 days in the presence of 0.2 μM maraviroc, but the wild type could not. The concentration of maraviroc was increased up to 0.7 μM for HIV-1_{V3Lib} and up to 0.1 μM for HIV-$1_{JR-FL-P17}$ at passage 17.

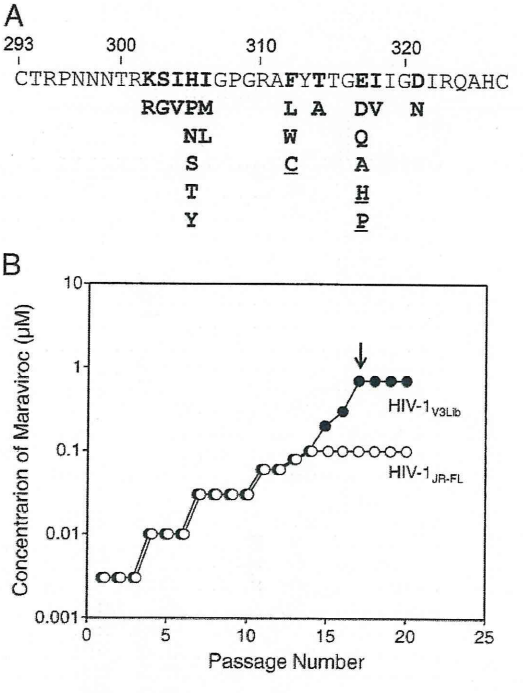

Fig. 1. (A) Amino acid substitutions in HIV-1_{V3Lib}. Residues in boldface indicate the substitutions that were randomly incorporated in HIV-1_{V3Lib}. Underlined residues indicate the substitutions that were not detected in 31 R5 viruses (Yusa et al., 2005). F312C, E317H, and E317P were inevitably incorporated in HIV-1_{V3Lib} due to combinations of nucleotide substitutions. (B) Induction of maraviroc-resistant variants from HIV-1_{V3Lib}. HIV-1_{JR-FL} and HIV-1_{V3Lib} were passaged in PM1/CCR5 cells in the presence of maraviroc increasing from 0.003 μM to 0.1 μM for HIV-1_{JR-FL} and from 0.003 μM to 0.7 μM for HIV-1_{V3Lib}.

We determined the drug susceptibilities in the passaged viruses (Table 1). HIV-$1_{JR-FL-P17}$ revealed an 8-fold higher resistance than the wild type without drug selection. It should be noted that replication of HIV-$1_{V3Lib-P17}$ could not be blocked with even 10 μM of maraviroc, indicating that HIV-$1_{V3Lib-P17}$ was >1449-fold more resistant than the wild type with selection. HIV-$1_{V3Lib-P17}$ could replicate at extremely high concentrations of maraviroc; we designated this full resistance as complete resistance. Furthermore, HIV-$1_{V3Lib-P17}$ revealed a cross-resistance of >230-fold to TAK-779, although HIV-$1_{JR-FL-P17}$ showed only a 3.5-fold resistance compared with the wild type without selection. These results suggested that a certain intrinsic change occurred in HIV-1_{V3Lib} after passage 14. The viral fitness of HIV-$1_{JR-FL-P17}$ and HIV-$1_{V3Lib-P17}$ was compared with that of viruses without selection by measuring p24 Gag in the supernatant (Fig. 2A). Before selection with maraviroc, HIV-1_{V3Lib} revealed lower fitness than HIV-1_{JR-FL}. Replication of HIV-$1_{JR-FL-P17}$ was almost comparable to that of HIV-1_{JR-FL}, while the viral fitness of HIV-$1_{V3Lib-P17}$ was higher than that of HIV-1_{JR-FL} or HIV-1_{V3Lib} on day 2 or 4. These results indicated that not only more resistant but also more fitness-adapted variants dominantly overgrew during the passages for selection.

HIV-1_{V3Lib} did not inherently contain V3 mutants that could use CXCR4 as a coreceptor (Yusa et al., 2005). To address whether coreceptor switching occurred in HIV-$1_{V3Lib-P17}$, MT-2 cells, which could support X4 virus HIV-1_{NL4-3} but not R5 virus HIV-1_{JR-FL} (Fig. 2B), were infected with the virus. It was clearly shown that HIV-$1_{V3Lib-P17}$ could not replicate in MT-2 cells using CXCR4, indicating that the high resistance to maraviroc in HIV-$1_{V3Lib-P17}$ was not due to coreceptor switching.

Mutations in HIV-$1_{JR-FL-P17}$ and HIV-$1_{V3Lib-P17}$ at passage 17

To identify the mutations responsible for complete resistance to maraviroc, we sequenced *env* genes at passage 10 and 17 (Table 2). At passage 10, S303G was partially detected in HIV-$1_{JR-FL-P10}$ gp120 by direct sequencing. Actually, 2 of 4 clones of HIV-$1_{JR-FL-P10}$ contained S303G alone in the V3 loop, and no other common mutations were detected in the other regions of gp120 and gp41 (data not shown). Virus clones containing S303G did not become a major population after further selection at passage 17. T314P (4 of 8 clones), S303G (2 of 8 clones), N299S (2 of 8 clones), K302E (1 of 8 clones), and A311L (1 of 8 clones) were detected in the V3 loop, indicating that the V3

Table 1
Susceptibility of the viruses selected with maraviroc.

	EC_{50}[a] (μM)	
	Maraviroc[b]	TAK-779[b]
HIV-1_{JR-FL}	0.0069 ± 0.0019[c] (1.0)	0.043 ± 0.009 (1.0)
HIV-$1_{JR-FL-P17}$	0.055 ± 0.0055 (8.0)	0.15 ± 0.033 (3.5)
HIV-1_{V3Lib}	0.0055 ± 0.0007 (0.80)	0.025 ± 0.007 (0.58)
HIV-$1_{V3Lib-P17}$	>10 (>1400)	>10 (>230)

[a] PM1/CCR5 cells were infected at 100 TCID50 of viruses in the presence of the CCR5 inhibitor on day 0. Cytopathic effect was determined on day 6 by MTT method.
[b] Drug concentration of 50% growth inhibition of the cells (CC50) was >10 μM.
[c] Mean ± SD (n = 3).

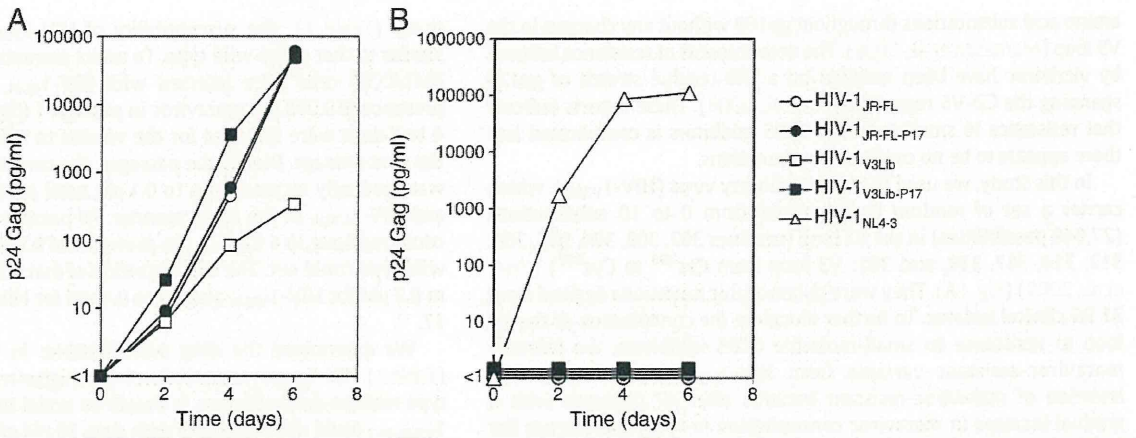

Fig. 2. Replication of HIV-$1_{JR\text{-}FL\text{-}P17}$ and HIV-$1_{V3Lib\text{-}P17}$ in PM1/CCR5 cells (A) or MT2 cells (B). Cells (5×10^4) were infected with 10 ng of p24 Gag. Viral replication was monitored by measuring p24 Gag in the supernatant. Experiments were performed in triplicate.

structure was not strictly focused on the selection pressure. Instead, T199K in the C2 region was the only mutation detected by direct sequencing, and the mutation was confirmed in 7 of 8 clones. The mixture of these clones (HIV-$1_{JR\text{-}FL\text{-}P17}$) revealed 8-fold resistance to maraviroc (Table 1), suggesting that T199K may be a responsible mutation for the low resistance in HIV-$1_{JR\text{-}FL\text{-}P17}$.

The mutation profile of HIV-1_{V3Lib} at passage 10 was different from that at passage 17. In passage 10, S303G (4 of 4), I306M (3 of 4), F312W (3 of 4), T314A (3 of 4), and I322N (4 of 4) were detected in a major population, and 1 of 4 clones contained G149R/T199A in the non-V3 region. Thus, suggesting that the low concentrations of maraviroc from 0.003 to 0.01 μM compelled the condensation of the V3-mutant mixture to a small number of V3 structures. After further selection, the V3 structures detected in passage 10 were lost at passage 17, and 5 mutations in the V3 loop, I304V/F312W/T314A/E317D/I318V (designated as V3-M5) and T199K/T275M (all 8) were detected by direct sequencing. The amino acid substitutions of V3-M5 were polymorphic mutations inherently incorporated into the library virus. All of the clones from HIV-$1_{V3Lib\text{-}P17}$ contained these 7 common mutations, although some of them contained minor mutations such as T262L (3 of 8). There were no other mutations detected in the other regions of gp120 and gp41 (data not shown). HIV-$1_{V3Lib\text{-}P17}$ revealed a >1400-fold

Table 2
Mutations in gp120 of V3 loop library virus selected with maraviroc.

maraviroc (μM)	non-V3 mutations	V3 mutations[a]
		293 300 310 320
HIV-$1_{JR\text{-}FL}$		CTRPNNNTRKSIHIGPGRAFYTTGEIIGDIRQAHC
P10[b] 0.03	**-**	.....**G**.....
CL#01	D227V	.....G.....
CL#02	-	.....
CL#03	V267I	.....G.....
CL#04	Y174H/T199K	.....
P17[b] 0.1	**T199K**	.....**P**.....
CL#01	L124F/V197A/T199K/E220L/S240G	.....P.....
CL#02	V83L/N87Y/T199K/G442E	.....P.....
CL#03	V83I/T199K/C436R/N452D	.....P.....
CL#04	V83L/T199K/F378Y	.....P.....
CL#05	V166A/T199K/P209L/L256R/N351D	.....G.....L.....
CL#06	-	.....S.....
CL#07	N140D/T199K	.....S.....
CL#08	N134I/T199K/K233E	.....EG.....
HIV-$1_{JR\text{-}FL\text{-}V3Lib}$		
P10 0.03	**-**	.....**G..M.....W.A.....N**.....
CL#01	-	.....G..M.....W.A.....N.....
CL#02	G149R/T199A	.....G..M.....L.A..A...N.....
CL#03	-	.....G..M.....W.A.....N.....
CL#04	-	.....GV.L.....W....Q...N.....
P17 0.7	**T199K, T275M**	.....**V.....W.A..DV**.....
CL#01	T199K/T275M	.....V.....W.A..DV.....
CL#02	T199K/T275M	.....V.....W.A..DV.....
CL#03	T199K/T275M	.....V.....W.A..DV.....
CL#04	T199K/E265K/T275M	.....V.....W.A..DV.....
CL#05	T199K/T262L/T275M	.....V.....GW.A..DV.....
CL#06	T199K/E208K/G219S/T262L/T275M	.....V.....W.A..DV.....
CL#07	T199K/T262L/T275M	.....V.....W.A..DV.....
CL#08	T199K/T275M	.....V.....W.A..DV.....

[a] Amino acid residues underlined are the mutation positions in HIV-$1_{JR\text{-}FL\text{-}V3Lib}$.
[b] P10, P17 direct sequencing was performed to detect mutations (in bold) in Env.

resistance to maraviroc compared with HIV-1_{JR-FL} (Table 1). These results strongly suggested that T199K/T275M plus V3-M5 conferred complete resistance to maraviroc.

Susceptibilities of recombinant viruses to maraviroc

To confirm which mutations were responsible for complete resistance, we constructed molecular clones containing combinations of T199K, T275M, and/or V3-M5, and measured their susceptibilities to maraviroc (Fig. 3). EC_{50} of HIV-1_{JR-FL} was 0.018 ± 0.004 μM, while those of HIV-1_{T199K} and HIV-1_{T275M} were 0.042 ± 0.007 μM and 0.074 ± 0.011 μM. Thus HIV-1_{T199K} and HIV-1_{T275M} were 2.3- and 4.1-fold more resistant than HIV-1_{JR-FL}. HIV-$1_{T199K/T275M}$ was 3.3-fold more resistant, indicating that without V3 mutations, T199K, T275M, or T199K/T275M could confer low resistance, but not lead to complete resistance. On the other hand, the V3-M5 alone could confer complete resistance to maraviroc, although its viral fitness was lower than that of HIV-1_{JR-FL} (Fig. 4). p24 Gag produced in the absence of maraviroc in HIV-1_{V3-M5} was 1040 pg/ml and that in HIV-1_{JR-FL} was 8600 pg/ml. T199K combined with V3-M5 can confer complete resistance, and increase its viral fitness. p24 Gag production in HIV-$1_{T199K/V3-M5}$ in the absence of maraviroc was 8.5-fold higher than that in HIV-1_{V3-M5}. T275M was detected in all 8 clones at passage 17, however, the combination of T275M with V3-M5 resulted in marked decrease of viral fitness (Fig. 4), although the viral replication could not be suppressed by 3 or 10 μM maraviroc. These results indicated that T275M with V3-M5 could confer complete resistance. T275M/V3-M5 plus T199K restored the decreased viral fitness with complete resistance. The replication of HIV-$1_{T199K/T275M/V3-M5}$ in the presence of 3 or 10 μM maraviroc was comparable to that of HIV-1_{JR-FL}. Taken together, V3-M5 is responsible for the acquisition of complete resistance, and T199K and/or T275M have a strong effect on viral replication under drug selection pressure.

Susceptibilities of pseudotyped viruses: single-round entry assay

To confirm the noncompetitive resistance mechanism, we determined the susceptibilities of the recombinant viruses with a single-round entry assay using MAGIC-5 cells (Hachiya et al., 2001). EC_{50} of pseudotyped HIV-$1_{Env-JR-FL}$ was 0.00035 ± 0.00007 μM. The pseudotyped viruses HIV-$1_{Env-T199K/T275M/V3-M5}$, HIV-$1_{Env-T199K}$, HIV-$1_{Env-T275M}$, HIV-$1_{Env-T199K/T275M}$, HIV-$1_{Env-V3-M5}$, HIV-$1_{Env-T199K/V3-M5}$, and HIV-$1_{Env-T275M/V3-M5}$ revealed a ≤3.4-fold resistance compared with HIV-$1_{Env-JR-FL}$. The competent molecular clones containing T199K/T275M/V3-M5, V3-M5, T199K/V3-M5, and T275M/V3-M5 could not be blocked by 3 or 10 μM maraviroc (Fig. 4), while single-round entry of these pseudotyped viruses could be inhibited by 50% with ≤0.0012 μM of maraviroc (Table 3). However, in the presence of 0.1 or 1 μM maraviroc, inhibition of viral entry could not be completely blocked (Fig. 5), indicating that the viruses could utilize the maraviroc-bound form of CCR5. HIV-1_{V3-M5}, HIV-$1_{T199K/V3-M5}$, and HIV-$1_{T199K/T275M/V3-M5}$ retained 19, 26, and 36%, respectively, of their entry ability at 1 μM maraviroc than those of the pseudotyped virus in drug-free conditions. These results indicated that these viruses acquired noncompetitive resistance by interacting with the maraviroc-binding CCR5 complex as a second receptor.

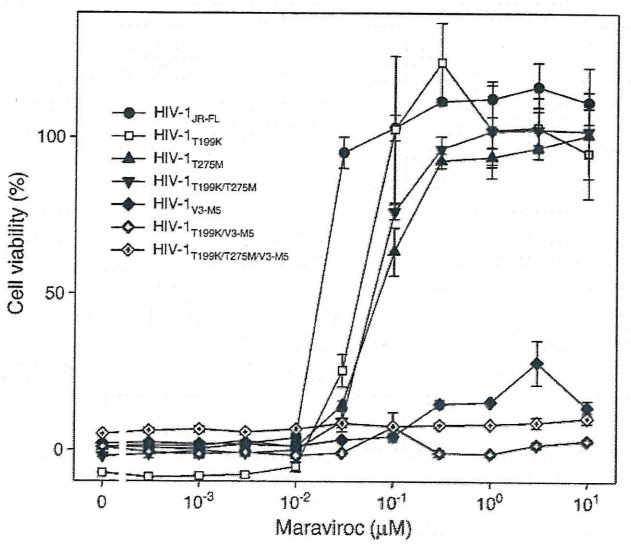

Fig. 3. Susceptibilities of replication-competent recombinant viruses. PM1/CCR5 cells were infected with recombinant virus at 100 $TCID_{50}$ in the presence of maraviroc and cultured for 6 days, and the cytopathic effect was determined by the MTT assay. Susceptibility of HIV-$1_{T275M/V3-M5}$ could not be examined because of its low replication. Mean ± SD (n = 3).

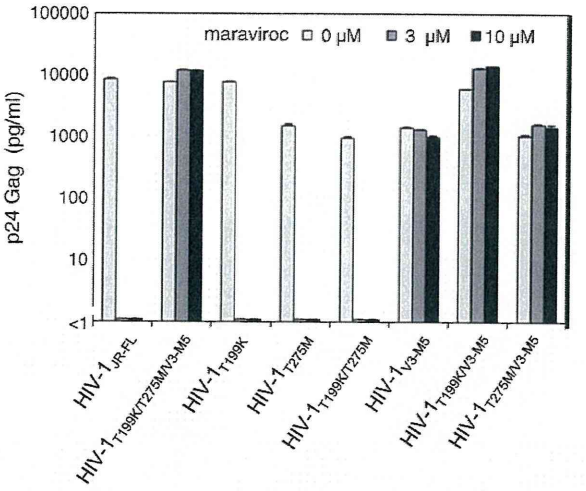

Fig. 4. The effect of 3 or 10 μM of maraviroc on the production of p24 Gag in the recombinant viruses. Cells (5×10^4) were infected with 10 ng of p24 Gag in the presence of 3 or 10 μM of maraviroc. After 6 days, the amount of p24 Gag in the supernatant was measured with HIV-1 p24 Gag ELISA. Mean ± SD (n = 3).

Discussion

Maraviroc is a highly potent antiviral agent targeting CCR5 to block the viral entry step (Kuhmann and Hartley, 2008; MacArthur and Novak, 2008). Primary R5 isolates cultured in stimulated PBMC are usually used to induce CCR5 inhibitor-resistant variants (Baba et al., 2007; Kuhmann et al., 2004; Marozsan et al., 2005; Ogert et al., 2008; Pugach et al., 2007; Trkola et al., 2002; Westby et al., 2007). Here we used PM1/CCR5 cells with the HIV-1_{V3Lib} constructed from a laboratory strain to further focus on the contribution of the V3 loop in gp120 in acquisition of maraviroc resistance. If HIV-1_{V3Lib} originally contained maraviroc-resistant viruses without additional mutations,

Table 3
Susceptibility of recombinant viruses to maraviroc determined by single-round entry assay.

	Maraviroc	
	EC_{50}[a]	(μM)
HIV-$1_{Env-JR-FL}$	0.00035 ± 0.00007[b]	(1.0)
HIV-$1_{Env-T199K/T275M/V3-M5}$	0.00090 ± 0.00014	(2.6)
HIV-$1_{Env-T199K}$	0.00050 ± 0.00007	(1.4)
HIV-$1_{Env-T275M}$	0.00085 ± 0.00015	(2.4)
HIV-$1_{Env-T199K/T275M}$	0.00064 ± 0.00018	(2.6)
HIV-$1_{Env-V3-M5}$	0.00071 ± 0.00022	(2.0)
HIV-$1_{Env-T199K/V3-M5}$	0.0012 ± 0.0005	(3.4)
HIV-$1_{Env-T275M/V3-M5}$	0.00064 ± 0.00021	(1.8)

[a] MAGIC-5 cells (2 x 10^4) were infected with pseudotyped virus on day 0, and 48 h postinfection luciferase activity was measured to determine effective concentration of 50% entry inhibition (EC_{50}).
[b] Mean ± SD (n = 3).